AUTHOR(S)
Fan, L., Zhang, X., Wang, L., Song, Y., Yi, K., Wang, X., Zhang, H., Li, L., & Zhao, Y.

TITLE
Bio-Inspired Porous Microneedles Dwelled Stem Cells for Diabetic Wound Treatment

YEAR
2024

DOI
10.1002/adfm.202316742

CITATION
Fan, L., Zhang, X., Wang, L., Song, Y., Yi, K., Wang, X., Zhang, H., Li, L., & Zhao, Y. (2024). Bio-Inspired Porous Microneedles Dwelled Stem Cells for Diabetic Wound Treatment. *Advanced Functional Materials*, 34(28). Portico. https://doi.org/10.1002/adfm.202316742

VERSION
Accepted Manuscript

Bio-inspired porous microneedles dwelled stem cells for diabetic wound treatment

Lu Fan, Xiaoxuan Zhang, Li Wang, Yizuo Song, Kexin Yi, Xiaoju Wang, Hongbo Zhang *, Ling Li*, Yuanjin Zhao*

Dr. L. Fan, Dr. L. Wang, Dr. Y. Z. Song, Prof. H. B. Zhang, Prof. Y. J. Zhao.
Department of General Surgery, The First Affiliated Hospital of Wenzhou Medical University, Wenzhou, China
E-mail: yjzhao@seu.edu.cn

Dr. L. Fan, Dr. L. Wang, Dr. K. X. Yi, Dr. X. J. Wang, Prof. H. B. Zhang.
Pharmaceutical Sciences Laboratory, Åbo Akademi University, Turku 20520, Finland
E-mail: hongbo.zhang@abo.fi

Prof. L. Li
Department of Endocrinology, Zhongda Hospital, School of Medicine, Southeast University Nanjing 210009, China
E-mail: lingli@seu.edu.cn

Dr. X. X. Zhang, Prof. Y. J. Zhao.
Department of Rheumatology and Immunology, Nanjing Drum Tower Hospital, School of Biological Science and Medical Engineering, Southeast University, Nanjing 210096, China

Prof. H. B. Zhang
Turku Bioscience Centre, University of Turku and Åbo Akademi University, Turku 20520, Finland

Keywords: bioinspired, microneedle, hydrogel, stem cell, niche, diabetic wound

Diabetic wound healing is a serious, complex, and chronic process; one current promising and focusing technology in this area is stem cell treatment. Here, we fabricated novel porous microneedle (MN) arrays, which can highly mimetic stem cell niches, through template filling and particle etching method. The human adipose-derived stem cells (ADSCs) are encapsulated in Matrigel then loaded into the porous MN arrays by post-perfusion. Because of the extracellular matrix-mimicking, the biocompatible Matrigel offers a bionic microenvironment of stem cell nest suitable for growth. Benefiting from the numerous pore structures of MNs, the loaded ADSCs have enough space to fully absorb nutrients, proliferate greatly and exhibit prompted function. In addition, the cell-loaded MN arrays have enough mechanical strength to penetrate the skin, allowing the ADSCs to get into the deep wound

areas. Based on these features, we have demonstrated the performance of the resultant MN arrays in promoting tissue regeneration, collagen deposition and angiogenesis in diabetes wounds of rat models. Thus, we believe that the bioinspired porous MNs can act as excellent stem cell scaffolds and will find many practical values in clinic wound healing.

1. Introduction

Diabetic wounds are usually with a serious and complex disorder featured by delayed healing.[1–4] They could induce infection and even amputation, which greatly lead to financial and therapeutic burdens.[5–7] Therapies for diabetic wounds contain ulcer debridement, tissue perfusion and cell transplantation.[8–10] Among them, stem cell-based transplantation strategy is considered to pull the wound healing treatment into a new stage[11–13], as they can secrete various bioactive factors and own the ability to promote tissue regeneration and immune regulation.[14–16] In particular, human adipose-derived stem cells (ADSCs) have received tremendous attention due to their abundant availability and easy accessibility.[17,18] However, the direct application of ADSCs faces ongoing challenges associated with cell inactivation[19,20], posing significant impediments to practical clinics. Although the hydrogel encapsulation of ADSCs for topic applications have achieved some improvements[21–23], most of these hydrogels exist complex chemical reactions and cannot provide a pleasant micro-ecological environment.[17,24] In addition, during the wound healing process, the formation of scab or epithelialization results in skin hardening[25–27], making them difficult for stem cells to reach and exert therapeutic effects at the subcutaneous damaged site, which greatly hinders the recovery of the wound. Thus, new strategies to enhance stem cell therapy for wound healing are yet to be explored.

Herein, inspired by the microstructure and microenvironment of stem cell niches, we proposed novel porous microneedles (MN) arrays with hydrogel-encapsulated stem cells post-

perfusion for diabetic wound treatment, as schemed in **Figure 1**. Stem cell niches serve as specialized microenvironments where stem cells reside and receive support for their self-renewal and vitality maintenance.[28–31] Such niches play a crucial role in regulating stem cell behaviour and fate determination, providing a conducive environment for their survival and function.[32,33] Besides, MN arrays, typically composed of a supportive substrate and organized micro-sized needles[34–36], offer a painless and non-intrusive method for drug delivery, which is attributed to their capability to create microscale channels in the skin without direct contact with nerve fibers and capillaries.[37,38] Given these advantages, it is conceivable that the combination of the unique properties of stem cell niches and MN arrays could establish an effective approach for stem cell therapy in wound healing.

In this paper, we fabricated the desired porous MN arrays with ADSCs hydrogel delivery by a combined template filling, particle etching and post-perfusion method to treat diabetic wounds. The porous MN arrays were fabricated by simply using UV-curable gelatin methacryloyl (GelMA) and poly(ethylene glycol) diacrylate (PEGDA) hybrid mixed with glass microspheres to fill negative molds, followed by overnight etching. The stem cells were loaded by perfusing ADSCs-encapsulated Matrigel into the porous MN arrays. This biocompatible Matrigel mimicked the extracellular matrix and thus could simulate the microenvironment of the stem cell nest suitable for ADSCs growth. Benefiting from the large number of holes scattered on porous MN arrays, ADSCs have enough space to fully absorb nutrients, proliferate greatly and exhibit prompting functions to secrete factors. Additionally, the MN arrays have sufficient mechanical strength for effective skin penetration, facilitating the contact of ADSCs and the wound areas. Based on these features, we have demonstrated in rat experiments that the proposed ADSCs-loaded MN arrays could promote tissue regeneration, collagen deposition and angiogenesis in diabetes wounds, indicating that they could be a promising therapy for clinical wound healing treatment.

2. Results and Discussion

In a typical experiment, the fabrication of porous MN arrays was achieved by template replication and particle etching methods. As shown in **Figure 2a**, gelatin methacryloyl (GelMA) solution and poly(ethylene glycol) diacrylate (PEGDA) mixed with glass microspheres was stuffed to PDMS negative mold, followed by adding back solution without glass microspheres. After UV solidification and final demold, the resultant MNs were immersed in hydrofluoric acid (HF) solution overnight. Then, by rinsing multiple times with ethanol and phosphate buffered saline (PBS), the porous MN arrays were finally obtained. Each MN displayed a conical shape, featuring a base diameter of 380 μm, a height of 830 μm and pore sizes of 50 μm. The height of MN tip is comparable to the thickness of most biomaterials applied in clinical wound healing. Meanwhile, it does not interfere with the granulation tissue formation during wound repair and not disrupt the underlying tissue layers. Additionally, to provide sufficient space for cell encapsulation, the diameter tips falls within the range of 300-500 μm. While the pore sizes ranging from 30 to 70 μm provide ample space for the growth, proliferation, migration, and metabolism of encapsulated ADSCs.

Morphology characterization showed that the solid MNs without porous structure had a smooth surface (**Figure 2b, c**). In comparison, the porous MNs before and after etching both had a rougher surface under the optical microscope, owing to numerous glass microspheres and holes formed structure (**Figure S1, Figure 2d, e**). Besides, the swelling properties of solid and porous hydrogel were further assayed (**Figure S2)**. The scanning electron microscope (SEM) image further proved the roughness of the porous MNs was attributed to the presence of numerous pore structures on the surface (**Figure 2f**). Obviously, the cross-sectional SEM images exhibited a significant number of internal pore structures within tips (**Figure 2g, Figure S3**). Such pore structures provided enough space for cell survival and proliferation. It was revealed that the higher concentration of SiO_2 glass microspheres, the

more pores the needles had and meanwhile the lower mechanical strength (**Figure S4, 5**). Despite with numerous pore structures, porous MN arrays displayed a similar favorable morphology to solid MNs. To further investigate the shape of MNs, needle lengths and base diameters were analysed. Results found the distribution of tip lengths was about 800 μm and base diameters mainly 300 μm, indicating the relatively uniform size of MNs (**Figure 2h, i)**. Finally, mechanical testing results confirmed per porous tip could withstand 0.49 N, and the MNs patch pressed to pigskin left obviously insert imprints, demonstrating the ability to penetrate the skin (**Figure 2j, Figure S6**).

In order to ensure the vitality of the infused ADSCs, it was essential to verify the biocompatibility of porous MNs before perfusion (**Figure S7**). We co-cultured porous MNs extraction and NIH 3T3 cells for cytotoxicity experiment. Compared with the control group, the MNs group exhibited superior cell-compatibility. In order to infuse cells into the pores of the porous MNs and meanwhile reduce the damage of bubbles to cells, a slight vacuum device was used as shown in **Figure S8**. Via a micro-negative pressure system, Matrigel containing ADSCs was infused into the pores of MNs (ADSCs-porous MNs) (**Figure 3a**). After that, the morphology of the whole MN arrays post-infusion was observed, and the shapes of tips were still complete (**Figure 3b**). Meanwhile, the compressive strength of per needle was a little higher than porous MNs before infusion, possibly because the Matrigel infusion assisted original tips to improve the mechanical strength (**Figure S9**).

Following cell infusion, the growth status of ADSCs on the MNs was assessed during 1, 3, 5, and 7 days of cultivation (**Figure 3c, d)**. With increasing culture days, the infused ADSCs significantly proliferated on porous MNs, indicating porous MNs could provide the normal growth and proliferation for cells (**Figure 3d**). Due to the high viscosity of the Matrigel, a small amount of ADSCs would adhere to the solid MN surface via mild vacuum. While, in comparison to solid MNs loaded ADSCs (ADSCs-solid MNs), quantitative statistics further demonstrated ADSCs on porous MNs exhibited a greater proliferation. (**Figure 3c**).

To investigate the distribution status of ADSCs dwelled on porous MNs, layer scanning was performed to observe the cell-loaded MNs after 7 days of cultivation (**Figure 3e**). Results indicated that ADSCs were primarily concentrated on the surface pores of porous MNs and had excellent growth in each layer. Finally, the cross-sectional image through SEM and fluorescence image also provided a top insight into the ADSCs-loaded MNs (**Figure 3f**). It was worth mentioning that the mixture of Matrigel and ADSCs only distributed in the outer layer of tips, possibly because a gentle vacuum was conducted to ensure cell viability. In addition, Matrigel with high viscosity decreases ADSCs amount pumped into the interior of MNs. Notably, not only ADSCs, but also adherent cells would have satisfactory proliferation and loading onto porous MNs via such perfusion strategy (**Figure S10**).

Vascular endothelial growth factor (VEGF) plays a crucial role in wound healing, especially in tissue restoration and remodelling. In order to investigate the biological function of ADSCs-MNs, we measured VEGF secretion of ADSCs-MNs by enzyme-linked immunosorbent assays (ELISA) at different cultivating days (**Figure 4a**). Results displayed that ADSCs dwelled on porous MNs exhibited successive VEGF secretion and had higher VEGF excretion than those on solid MNs on the 1^{st}, 3^{rd}, 5^{th} and 7^{th} days, owing to the higher number of dwelled ADSCs. Results demonstrated the efficacious VEGF secretion behaviour of ADSCs-porous MNs. To further confirm the ability of ADSCs-porous MNs to promote cell proliferation and migration, the scratch test was conducted by co-cultured the human umbilical vein endothelial cells (HUVECs) and leaching solution of MNs, ADSCs-solid MNs and ADSCs-porous MNs, respectively. After 24 hours, it was revealed that under equal initial scratch areas, the proliferation and migration rate of HUVECs treated with ADSCs-porous MNs extraction was much higher than those of MNs and ADSCs-solid MNs group (**Figure 4b, d**).

In addition, revascularization is vital for tissue repair by facilitating nutrients and oxygen supply. To confirm the ability of ADSCs-porous MNs to promote angiogenesis, a vessel

formation assay was performed by co-cultured HUVECs and the above material leaching solution. As a consequence, compared with other groups, HUVECs in ADSCs-porous MNs group exhibited the most obvious tubular structure and the highest number of meshes and junctions (**Figure 4c, e and f**), suggesting ADSCs-porous MNs owned robust vessel-forming ability. Conclusively, ADSCs dwelled on porous MNs could secrete effective concentrations of VEGF, promoting cell proliferation and migration, as well as revascularization.

In order to confirm the *in vivo* therapeutic efficacy of ADSCs-porous MNs, a diabetic wound rat model was established and cured in different manners. All rats were induced to enter a hyperglycemic state by intraperitoneal injection of streptomycin before creating a wound on their dorsal skin, and the treatment timeline was shown in **Figure 5a**. Subsequently, rats were randomly distributed into four groups and received different treatments: control, blank MNs, ADSCs-solid MNs, and ADSCs-porous MNs, respectively. During the healing process, we took photos over 0-10 days to monitor the changes in the wound area (**Figure 5b**). Results in the blank MNs group showed that the presence of MNs did not adversely affect on wound healing compared to control group. In fact, the therapeutic outcome of MNs group was slightly better than the control group, which possibly because the hydrogel provides a moist environment. While, rats in ADSCs-solid MNs group showed a relatively better therapeutic outcome than that of control and blank MNs, but inferior compared to ADSCs-porous MNs group, which possibly attributed to a lower ADSCs loaded and reduced VEGF secretion. Among these groups, ADSCs-porous MNs group exhibited the fastest healing rate up to 85% (**Figure 5c**). Results revealed that the proliferation and therapeutic function of ADSCs dwelled on porous MNs were superior to those on solid MNs, which were favorable for wound recovery.

Histological analysis is indispensable for analysing the therapeutic effect of ADSCs dwelled on porous MNs. Hematoxylin-eosin (H&E) staining was conducted to analyze the wound tissue formation on day 10 of treatment (**Figure 5d**). Compared with other groups,

ADSCs-porous MNs treated group significantly displayed the thickest dermal tissue (**Figure 5e**), suggesting superior tissue restoration for wound healing. Additionally, the deposition of collagen is an important indicator for wound healing. To access the growth and deposition of collagen fibers, Masson trichrome staining was performed on the wound bed (**Figure 6a**). It was found that rats in ADSCs-porous MNs group had denser collagen deposition and aligned fibers than any other groups (**Figure 6c**). Besides, CD31 serves as a marker for vascular endothelial cells, and angiogenesis is a critical step in wound healing. Through fluorescence staining, the ADSCs-porous MNs treated group displayed the best performance in neovascularization, with a significant increase in quantity and density (**Figure 6b, d**), demonstrating that ADSCs that dwelled on porous MNs produced growth factors that could induce neovascularization.

3. Conclusion

In summary, we have presented novel porous MN arrays with Matrigel-encapsulated stem cells post-perfusion for diabetic wound treatment. The porous MN arrays were fabricated by a combined template filling and particle etching method. The ADSCs have been loaded by perfusing the cell-encapsulated Matrigel into the porous MN arrays. Because of the extracellular matrix-mimicking, the biocompatible Matrigel offered a bionic microenvironment of the stem cell nest suitable for growth. It has been proved ADSCs dwelling on porous MNs had a greater proliferation and much more VEGF secretion than those on solid MNs, owning the ability to promote cell proliferation, migration and revascularization. In addition, the cell-loaded MN arrays have sufficient mechanical strength for effective skin penetration, allowing the ADSCs to get into the deep wound areas. Based on these features, we have demonstrated the performance of the resultant MN arrays in promoting tissue regeneration, collagen deposition and angiogenesis in diabetes wounds of rat

models. Thus, we are convinced that the bioinspired porous MNs can serve as excellent stem cell scaffolds and become a promising therapy for clinic wound healing.

4. Experimental section

Materials: SiO_2 glass spheres were bought from Fuhuanano Material. Gelatin methacryloyl (GelMA) was synthetized according to previous methods in the laboratory.[39] Lithium phenyl-2,4,6-trimethylbenzoylphosphinate (LAP), poly(ethylene glycol) diacrylate (PEGDA, average Mw ≈ 700), hydrofluoric acid (HF) and phosphate buffer (PBS) were purchased from Sigma-Aldrich. Cell Counting Kit-8 (CCK-8) was bought from Beyotime Biotech Inc. Calcein AM was bought from Thermo. Human adipose-derived stem cells (ADSCs) were from the American Type Culture Collection (ATCC). Matrigel was purchased from Corning. Ethanol was brought from Sinopharm Chemical Reagent.

Fabrication of Porous MNs: 30% GelMA, 5% PEGDA and 1‰ LAP were completely dissolved and then stored in the dark for subsequent use. After that, SiO_2 glass spheres with different concentrations (2%, 5% and 8%) were added to the prepolymer solution. Such thoroughly mixed solution was introduced into negative MN molds. Subsequently, the molds were placed in a vacuum pump to evacuate the gas within the MN cavities. Then, remove excessive patch solution and add PEGDA prepolymer solution as supporting base. After UV curing, GelMA@SiO_2 glass spheres MNs were demolded, followed by immersion in HF acid to etch the glass spheres in MN tips. After 12 hours, the resultant porous MNs were rinsed and soaked in ethanol and PBS multiple times to remove residual HF acid. The morphologies of the porous MNs and solid MNs without SiO_2 glass spheres were imaged under an optical microscope. The needle length and base diameter of the porous MNs were recorded. Additionally, the external surface and cross-sectional features of the porous MNs were observed via scanning electron microscopy (SEM). Image J software was used to analyze the pore size of MNs.

Fabrication of ADSCs-Porous/Solid MNs: ADSCs are digested from culture bottles and centrifuged for later use. Then, 0.5 mL Matrigel were added to ADSCs through gentle agitation to render uniform ADSCs dispersion. Subsequently, porous MNs were immersed in such mixture solution and they were placed into a mild micro-vacuum device for 10 min vacuum treatment, facilitating the infusion of the ADSCs mixture into the holes of porous MNs. After that, remove excess mixture solution and the porous MNs loaded ADSCs were retrieved and placed in a 37℃ incubator. Following an additional 10 min incubation, during which the Matrigel on MNs completely solidified, ADSCs-porous MNs (ADSCs amount of whole patch: 5×10^5) were transferred to a culture medium for further cultivation. Solid MNs without etching pores were loaded ADSCs (ADSCs-solid MNs) repeating the above procedure. Notably, 3T3 cells were also infused into the porous MNs via the same perfusion strategy, and 3T3 proliferation was observed under the fluorescence microscope. On the 1^{st}, 3^{rd}, 5^{th}, and 7^{th} days of cultivation, ADSCs viability was assessed using the CCK-8 assay, and cell proliferation was observed under a fluorescence microscope. On the 7^{th} day of cultivation, confocal layer scanning was employed to analyse ADSCs distribution on porous MNs, while SEM and fluorescence microscopy were utilized to record the top view of ADSCs-porous MNs.

Swelling properties: The swelling characteristics of porous and solid hydrogels were measured through swelling ratio. Dry hydrogel samples were immersed in PBS (pH = 7.4) at 37℃. At specific time points, the hydrogel samples were retrieved, rinsed with DI water, removed excess water, and then weighed. The swelling ratio was calculated using the following formula:

Swelling ratio = (Ws - Wd) / Wd × 100%,

where Ws and Wd represent the weights of swelling and dry hydrogel, respectively.

Mechanical Performance of Porous MNs: The mechanical characteristics of porous MNs were assessed utilizing a force analysis machine (HP-500, Handpi). MN patches with

different glass sphere concentrations (0, 2%, 5% and 8%) were positioned horizontally on the stable base, with the needle tips facing upward. Afterward, the force sensor was systematically brought closer to the tips in a vertical orientation. The sensor initiated measurements upon contact with the tips at a velocity of 0.2 mm s^{-1}. It stopped measurements until the tips were compressed. Repeating above process, the compressive force of the porous MNs perfused ADSCs-Matrigel was assessed. After the mechanical test, a porous MN patch was pressed on the pigskin by hand for 1 min and then removed. The image of imprints left on the pigskin surface after MNs insertion was recorded.

In Vitro Cytocompatibility Experiment: Cytocompatibility of porous MNs was evaluated by CCK-8 assay. Firstly, porous MNs were irradiated under UV light overnight. Subsequently, they were immersed in DMEM culture medium for 24 h to obtain the leaching solution. Then, 3T3 cells were cultured in the leaching solution for 3 days. Lastly, cell viability was assessed on days 1, 2, and 3 using CCK-8 assay, respectively.

Growth Factor Secretion Assessment: The quantification of vascular endothelial growth factor (VEGF) secretion by ADSCs was conducted through the enzyme-linked immunosorbent assay (ELISA). Both ADSCs-porous MNs and ADSCs-solid MNs were cultured for 7 days, and the supernatant was collected on the 1^{st}, 3^{rd}, 5^{th}, and 7^{th} day for measurement. The assay was performed by using the human VEGF-ELISA kit (Cusabio), following the instruction.

Scratch Assay: Human umbilical vein endothelial cells (HUVECs) were seeded onto a 6-well plate and cultured until they reached confluence. Then, scratches were made by using the tip of a pipette, followed by washing with PBS to remove detached cells. The HUVECs were then randomly divided into four groups: culture medium (Control), extracts from blank MNs (MN patches), extracts from solid microneedles loaded with cells (ADSCs-solid MNs), and extracts from porous microneedles perfused with ADSCs (ADSCs-porous MNs). After incubation for 0 and 24 h, photographs were taken to record the scratched areas, and then quantitative analysis was performed.

Tube Formation Assay: Initially, Matrigel was applied to a 48-well plate and then placed in a 37°C incubator. After complete solidification, HUVECs were seeded onto the Matrigel-coated plate until HUVECs adhered. The HUVECs were randomly divided into four groups and cultured in medium (Control), extracts from blank MNs (MN patches), extracts from solid microneedles loaded with cells (ADSCs-solid MNs), and extracts from porous microneedles perfused with ADSCs (ADSCs-porous MNs). After incubation for 4 h, the tube structure of each group was imaged under a microscope, and subsequent quantitative analysis was conducted.

In Vivo Treatment for Rat Models: To establish a type I diabetic rat model, streptozotocin (STZ) citrate buffer solution (50 mg/kg) was injected intraperitoneally into rats. All animal experiments were approved by the Animal Investigation Ethics Committee of Wenzhou Institute of University of Chinese Academy of Sciences (No.WIUCAS23021603). One week later, blood glucose levels of rats were measured. Once it was confirmed that the blood glucose levels in all rats were elevated to 11 mmol/L, rats were anesthetized with inhaled isoflurane and then circular full-thickness skin wounds measuring 1.5 cm in diameter were generated bilaterally on the dorsal aspect. Afterward, rats were randomly divided into four groups and received different treatments. The first group served as the control without treatment for wounds. The second group (MN patches) received blank porous MNs treatment without cell loading. The third group (ADSCs-solid MNs) was treated with solid MNs loaded with ADSCs. The fourth group (ADSCs-porous MNs) were treated with porous MNs dwelled with ADSCs. Before implantation, ADSCs-solid MNs and ADSCs-porous MNs was cultured for 7 days in the incubator. Wounds were taken photographs on days 3, 6, 8, and 10 of treatment. On the 10^{th} day, all rats were euthanized and wound tissues were collected, as well as histological staining (H&E and Mason staining) and immunofluorescence staining (CD31) were further performed.

Statistics Analysis: The control group as the standard for data normalization. All statistical analyses were conducted with Origin 2022 and Image J. Data were expressed as mean values ±standard deviation (SD). The Student' s t-test method was applied for evaluating the statistical significance. $P < 0.05$. $^{*}P < 0.05$, $^{**}P < 0.01$ and $^{***}P < 0.001$.

Supporting Information
Supporting Information is available from the Wiley Online Library or from the author.

Conflict of Interest
The authors declare no competing financial interests.

Acknowledgements
This work was supported by the Research Fellow (Grant No.353146), Project (347897), Solution for Health Profile (336355), and InFLAMES Flagship (337531) grants from Academy of Finland, Finland China Food and Health International Pilot Project funded by the Finnish Ministry of Education and Culture.

Author contributions
Y.J.Z., L.L. and H.B.Z. conceived the idea and designed experiments. L.F. conducted experiments and wrote the manuscript. X.X.Z assisted in data analysis, discussion and paper writing. W.L. and Y.Z.S. assisted in cell culture and animal experiments. W.L., Y.K.X. and W.X.J. revised the manuscript and checked the grammar.

Received: ((will be filled in by the editorial staff))
Revised: ((will be filled in by the editorial staff))
Published online: ((will be filled in by the editorial staff))

References

[1] S. Maschalidi, P. Mehrotra, B. N. Keçeli, H. K. L. De Cleene, K. Lecomte, R. Van der Cruyssen, P. Janssen, J. Pinney, G. van Loo, D. Elewaut, A. Massie, E. Hoste, K. S. Ravichandran, *Nature* **2022**, *606*, 776.
[2] V. Falanga, R. R. Isseroff, A. M. Soulika, M. Romanelli, D. Margolis, S. Kapp, M. Granick, K. Harding, *Nat Rev Dis Primers* **2022**, *8*, 1.
[3] G. Theocharidis, H. Yuk, H. Roh, L. Wang, I. Mezghani, J. Wu, A. Kafanas, M. Contreras, B. Sumpio, Z. Li, E. Wang, L. Chen, C. F. Guo, N. Jayaswal, X.-L. Katopodi, N. Kalavros, C. S. Nabzdyk, I. S. Vlachos, A. Veves, X. Zhao, *Nat. Biomed. Eng* **2022**, *6*, 1118.
[4] X. Ding, Y. Yu, W. Li, Y. Zhao, *Matter* **2023**, *6*, 1000.
[5] H. Cheng, Z. Shi, K. Yue, X. Huang, Y. Xu, C. Gao, Z. Yao, Y. S. Zhang, J. Wang, *Acta Biomaterialia* **2021**, *124*, 219.
[6] G. Chen, F. Wang, X. Zhang, Y. Shang, Y. Zhao, *Science Advances* **2023**, *9*, eadg3478.
[7] R. A. Mustafa, P. Parkkila, J. M. Rosenholm, H. Zhang, T. Viitala, *Smart Medicine* **2023**, *2*, e20230012.
[8] Y. Guan, H. Niu, Z. Liu, Y. Dang, J. Shen, M. Zayed, L. Ma, J. Guan, *Sci. Adv.* **2021**, *7*, eabj0153.

[9] M. Mirhaj, S. Labbaf, M. Tavakoli, A. M. Seifalian, *International Wound Journal* **2022**, *19*, 1934.
[10] E. Eriksson, P. Y. Liu, G. S. Schultz, M. M. Martins-Green, R. Tanaka, D. Weir, L. J. Gould, D. G. Armstrong, G. W. Gibbons, R. Wolcott, O. O. Olutoye, R. S. Kirsner, G. C. Gurtner, *Wound Repair Regen.* **2022**, *30*, 156.
[11] M. Hofer, M. P. Lutolf, *Nat Rev Mater* **2021**, *6*, 402.
[12] Z. Chen, Z. Lv, Y. Zhuang, Q. Saiding, W. Yang, W. Xiong, Z. Zhang, H. Chen, W. Cui, Y. Zhang, *Advanced Materials* **2023**, *35*, 2300180.
[13] C. M. Madl, S. C. Heilshorn, H. M. Blau, *Nature* **2018**, *557*, 335.
[14] R. Guillamat-Prats, *Cells* **2021**, *10*, 1729.
[15] R. Liu, B. Kong, J. Gan, Y. Zhao, L. Sun, *Chemical Engineering Journal* **2023**, *476*, 146608.
[16] S. Qian, J. Mao, Z. Liu, B. Zhao, Q. Zhao, B. Lu, L. Zhang, X. Mao, L. Cheng, W. Cui, Y. Zhang, X. Sun, *Smart Medicine* **2022**, *1*, e20220007.
[17] Y. Xu, X. Wu, X. Zhang, Y. Zu, Q. Tan, Y. Zhao, *Adv Funct Materials* **2023**, *33*, 2209986.
[18] N. Hu, Z. Cai, X. Jiang, C. Wang, T. Tang, T. Xu, H. Chen, X. Li, X. Du, W. Cui, *Acta Biomaterialia* **2023**, *157*, 175.
[19] Y. An, S. Lin, X. Tan, S. Zhu, F. Nie, Y. Zhen, L. Gu, C. Zhang, B. Wang, W. Wei, D. Li, J. Wu, *Cell Proliferation* **2021**, *54*, e12993.
[20] X. Zhang, H. Zhang, J. Gu, J. Zhang, H. Shi, H. Qian, D. Wang, W. Xu, J. Pan, H. A. Santos, *Advanced Materials* **2021**, *33*, 2005709.
[21] L. Ouyang, D. Qiu, X. Fu, A. Wu, P. Yang, Z. Yang, Q. Wang, L. Yan, R. Xiao, *Stem Cell Research & Therapy* **2022**, *13*, 395.
[22] S.-H. Wu, Y.-T. Liao, K.-K. Hsueh, H.-K. Huang, T.-M. Chen, E.-R. Chiang, S. Hsu, T.-C. Tseng, J.-P. Wang, *Frontiers in Cell and Developmental Biology* **2021**, *9*.
[23] S. Lee, D.-S. Chae, B.-W. Song, S. Lim, S. W. Kim, I.-K. Kim, K.-C. Hwang, *International Journal of Molecular Sciences* **2021**, *22*, 10586.
[24] S. Zhang, C. Qi, W. Zhang, H. Zhou, N. Wu, M. Yang, S. Meng, Z. Liu, T. Kong, *Advanced Materials* **2023**, *35*, 2209263.
[25] Z. Zhang, Z. Ni, Y. Huang, H. Zhang, Z. Hu, D. Ye, Y. Shen, M. Jia, K. Shi, G. Zhu, J. He, L. Xu, F. Shi, H. Yu, L. Zhuang, H. Wang, *ACS Appl. Mater. Interfaces* **2023**, *15*, 37214.
[26] H. Li, F. Cheng, X. Wei, X. Yi, S. Tang, Z. Wang, Y. S. Zhang, J. He, Y. Huang, *Materials Science and Engineering: C* **2021**, *118*, 111324.
[27] S. Hu, Z. Yang, Q. Zhai, D. Li, X. Zhu, Q. He, L. Li, R. D. Cannon, H. Wang, H. Tang, P. Ji, T. Chen, *Small* **2023**, *19*, 2207437.
[28] Z. Liu, X. Wan, Z. L. Wang, L. Li, *Advanced Materials* **2021**, *33*, 2007429.
[29] D. Bayik, J. D. Lathia, *Nat Rev Cancer* **2021**, *21*, 526.
[30] X. Lin, L. Fan, L. Wang, A. M. Filppula, Y. Yu, H. Zhang, *Smart Medicine* **2023**, *2*, e20230017.
[31] H. Chen, J. Guo, F. Bian, Y. Zhao, *Smart Medicine* **2022**, *1*, e20220001.
[32] X. Wu, H. Zhu, J. Che, Y. Xu, Q. Tan, Y. Zhao, *Bioactive Materials* **2023**, *26*, 159.
[33] H. Zhu, X. Wu, R. Liu, Y. Zhao, L. Sun, *Advanced Science* **2023**, *10*, 2206253.
[34] L. Fan, X. Zhang, X. Liu, B. Sun, L. Li, Y. Zhao, *Adv Healthcare Materials* **2021**, *10*, 2002249.
[35] L. Fan, X. Zhang, M. Nie, Y. Xu, Y. Wang, L. Shang, Y. Zhao, Y. Zhao, *Adv Funct Materials* **2022**, *32*, 2110746.
[36] X. Zhang, L. Sun, Y. Wang, F. Bian, Y. Wang, Y. Zhao, *Proceedings of the National Academy of Sciences* **2019**, *116*, 20863.
[37] S. Kusama, K. Sato, Y. Matsui, N. Kimura, H. Abe, S. Yoshida, M. Nishizawa, *Nat Commun* **2021**, *12*, 658.

[38] H. Chang, S. W. T. Chew, M. Zheng, D. C. S. Lio, C. Wiraja, Y. Mei, X. Ning, M. Cui, A. Than, P. Shi, D. Wang, K. Pu, P. Chen, H. Liu, C. Xu, *Nat Biomed Eng* **2021**, *5*, 1008.
[39] J. Yang, X. Wang, D. Wu, K. Yi, Y. Zhao, *Journal of Nanobiotechnology* **2023**, *21*, 178.

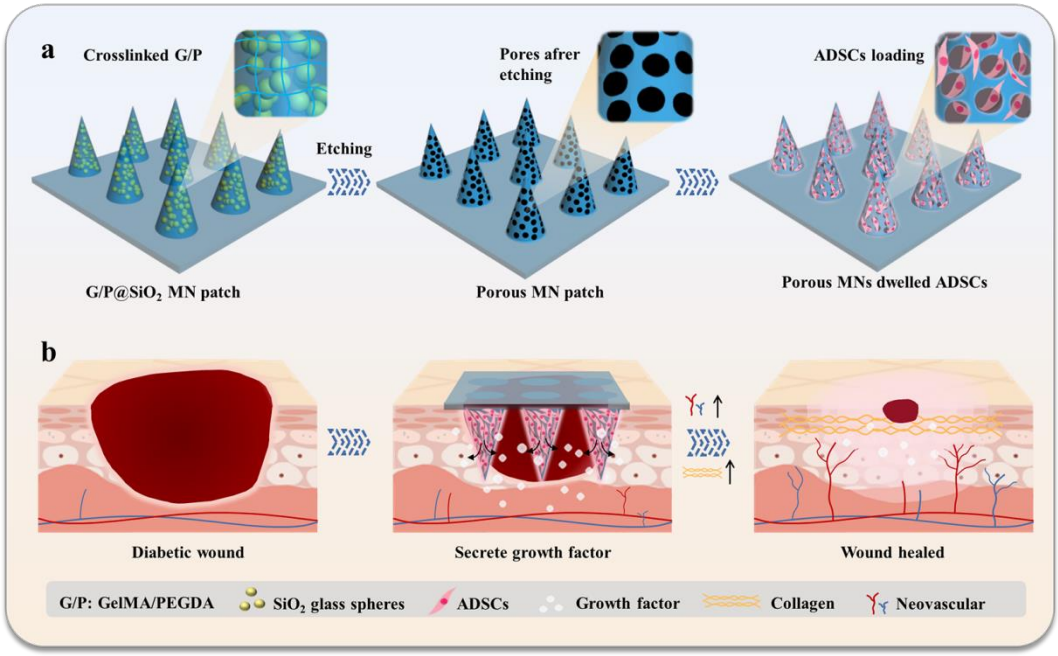

Figure 1. Schematic diagram of (a) the preparation of porous MNs loaded with ADSCs, and (b) its application in wound healing.

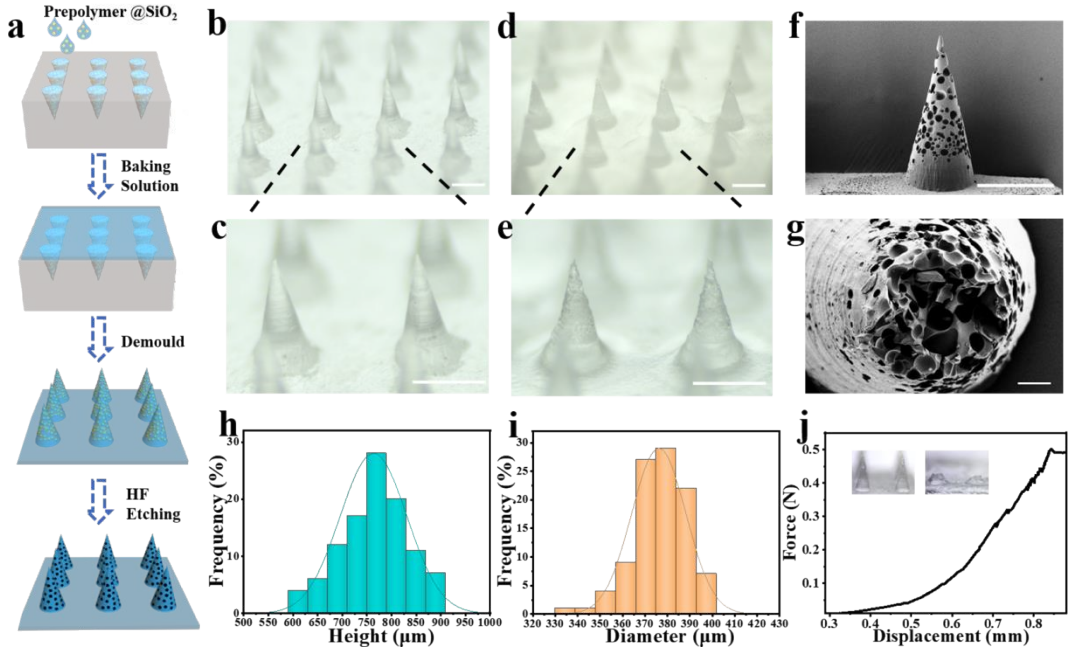

Figure 2. (a) Scheme of preparation process of porous MN arrays. (b) Solid MN array without SiO2 glass spheres etching and (c) local enlarged image; scale bars both are 400 μm. (d) Porous MN array after etching image and (e) local enlarged image; both scale bars are 400

μm. SEM images of (f) side view and (g) cross-sectional view of a needle; scale bar in (f) is 400 μm and in (g) is 50 μm. (h) Tip lengths statistics and (i) base diameters statistics of MN array. (j) Compressive strength of the porous MN array.

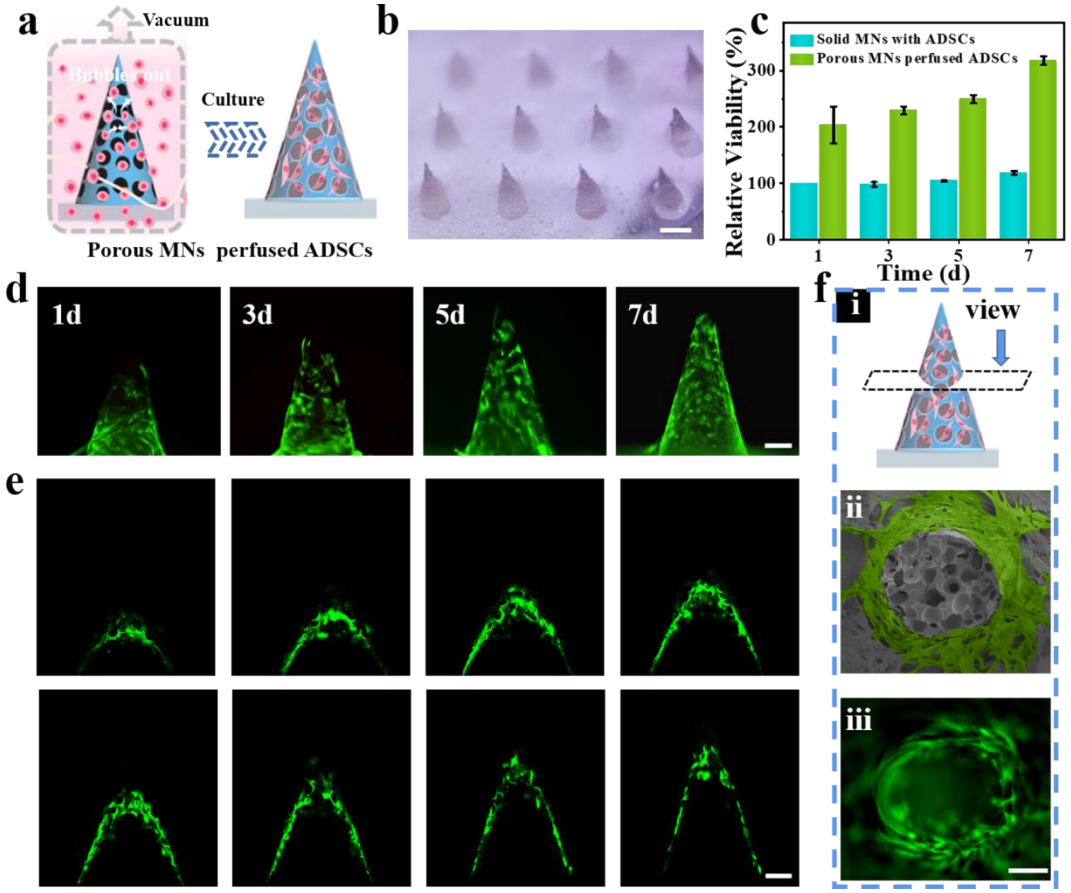

Figure 3. (a) Schematic diagram of the processes of porous MNs dwelled ADSCs. (b) Optical image of porous MN arrays infused with ADSCs; scale bar is 400 μm. (c) Statistics and (d) fluorescence staining of ADSCs proliferation activity on porous MNs on the 1st, 3rd, 5th and 7th days. Data are presented as mean ± SD (n = 3). (e) Confocal layer scanning images of porous MN arrays infused with ADSCs on the 7th day. (f) Top view schematic diagram (i), SEM pseudo color image (ii) and fluorescence image (iii) of ADSCs-porous MN arrays. Scale bars in (d), (e) and (f) are all 100 μm.

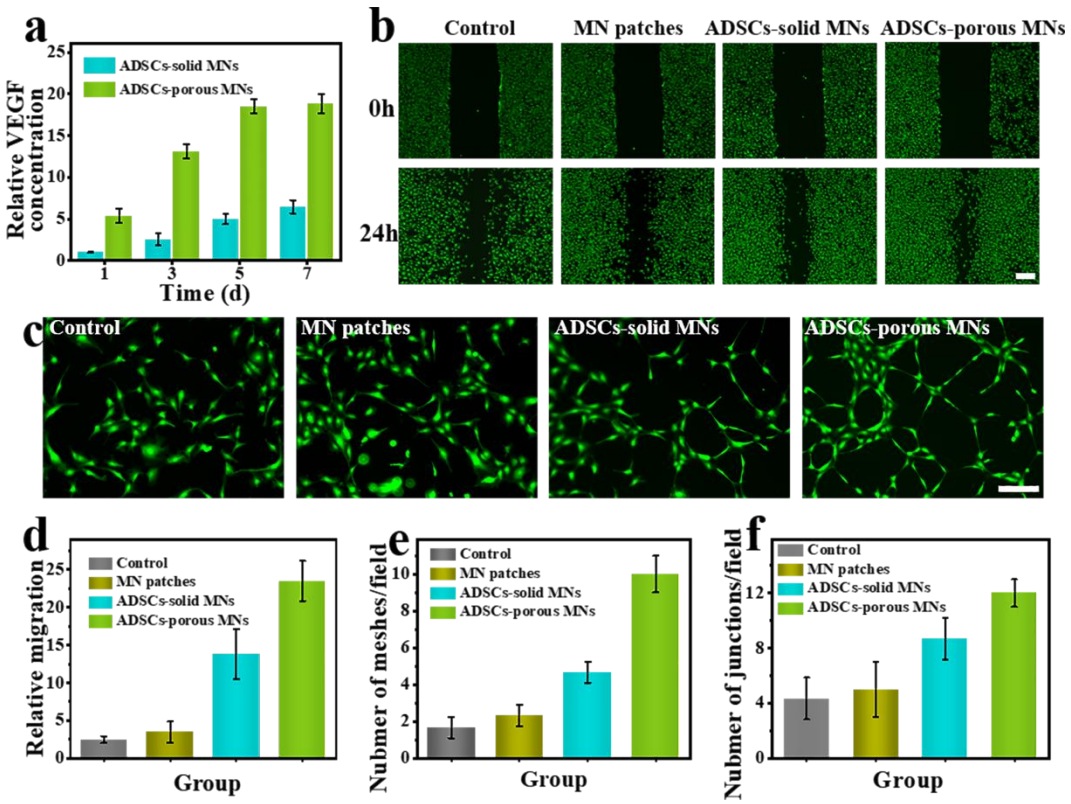

Figure 4. (a) VEGF release amount on different cultivation days. Relative to VEGF section of ADSCs-solid MNs group on 1st day. (b) Scratch test results between different groups for 0 and 24 hours; scale bar is 200 μm. (c) Vascular ring formation in different groups; scale bar is 50 μm. (d) Quantitative statistics of cell growth area after scratches. Relative to control group. (e) The number of blood vessels forming meshes and (f) junctions. Data are presented as mean ± SD (n = 3).

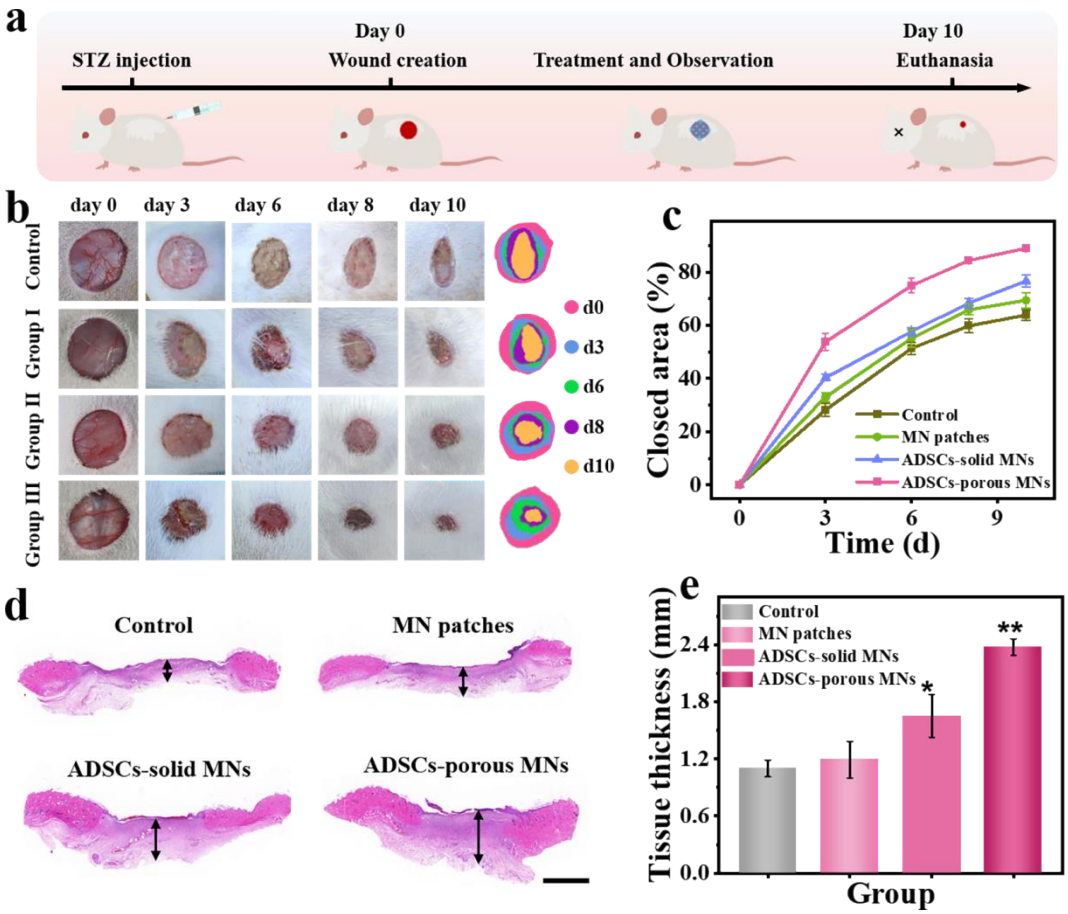

Figure 5. (a) Schematic description and timeline for animal experiment. (b) Wound recovery on different days and groups and simulation of the wound surface. (c) Statistics of wound closure area on different days. (d) H&E staining of wounds between different groups; scale bar is 2 mm. (e) Quantitative analysis of tissue thickness in different groups. **P < 0.05, **P < 0.01 and ***P < 0.001*. Data are presented as mean ± SD (n = 5).

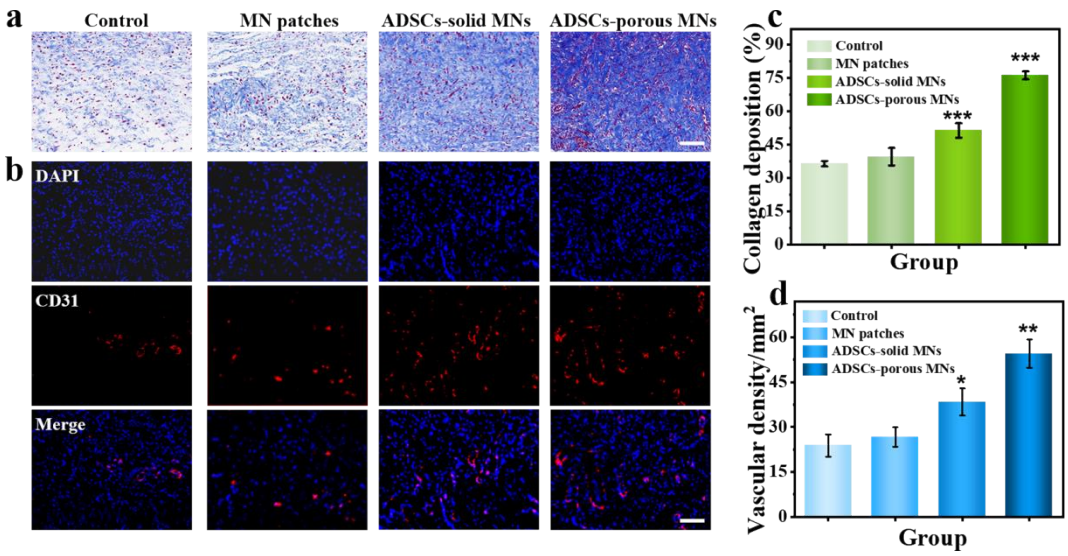

Figure 6. (a) Masson staining and (b) Immunofluorescence staining of different group rats wound beds on day 10. Both scale bars are 100 μm. (c) Quantitative analysis of collage

deposition and (d) vascular density in different groups. *$P < 0.05$, **$P < 0.01$ and ***$P < 0.001$. Data are presented as mean ± SD (n = 5).

Supporting Information

Bio-inspired porous microneedles dwelled stem cells for diabetic wound treatment

Lu Fan, Xiaoxuan Zhang, Li Wang, Yizuo Song, Kexin Yi, Xiaoju Wang, Hongbo Zhang *, Ling Li*, Yuanjin Zhao*

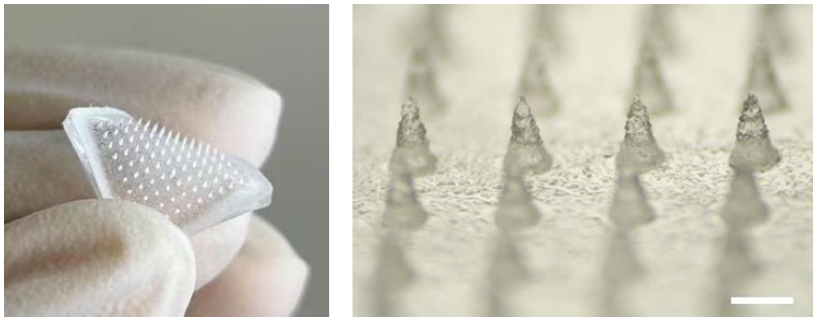

Figure S1. Optical images of GelMA@SiO_2 microneedles (before etching); scale bar is 400 μm.

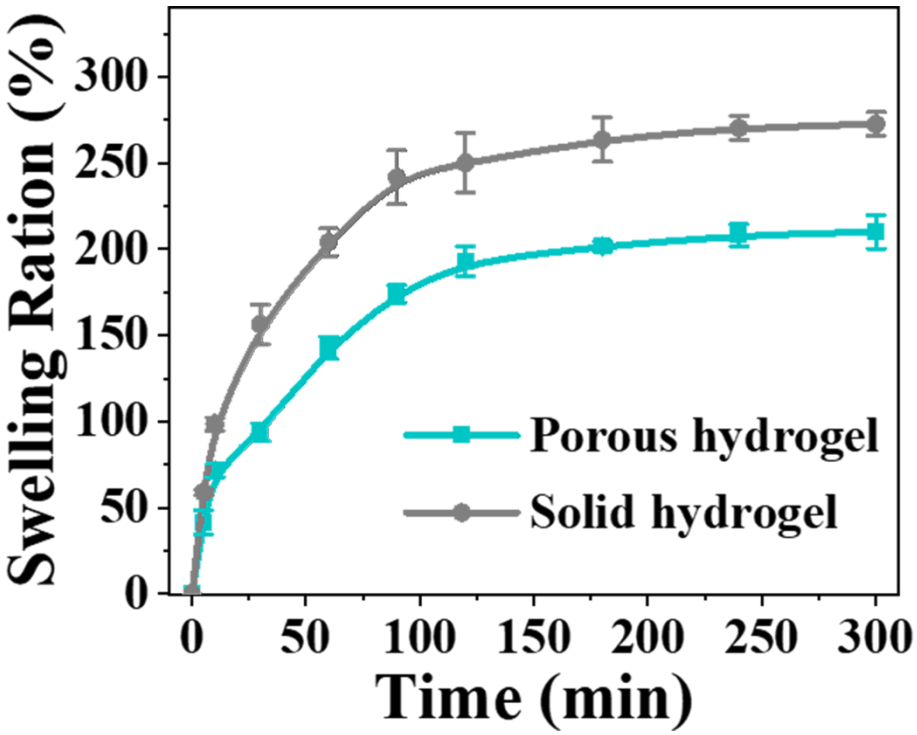

Figure S2. Swelling ration of porous and solid hydrogel in PBS. Data are presented as mean ± SD (n = 3).

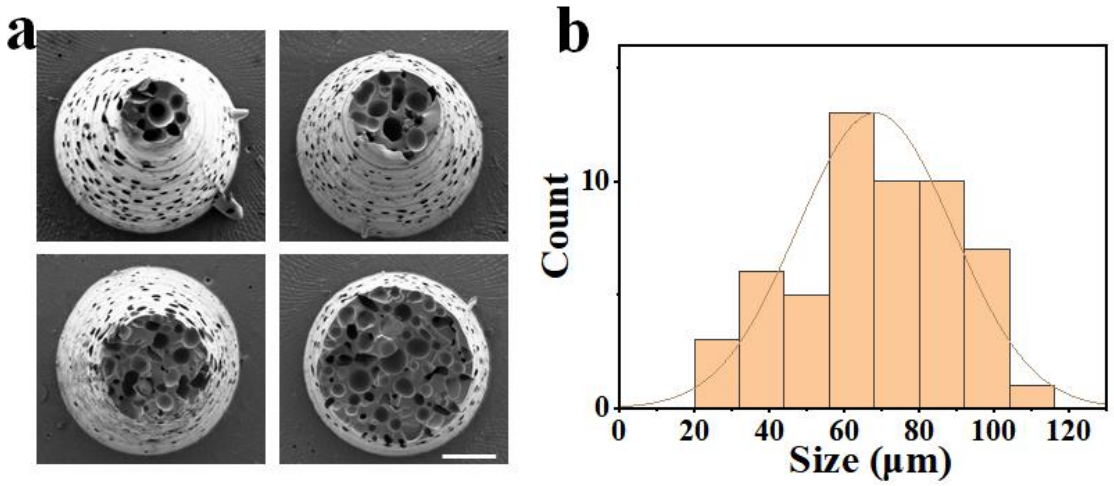

Figure S3. (a) SEM images of cross sections of porous MNs at different heights; scale bar is 100 μm. (b) Pore size statistics.

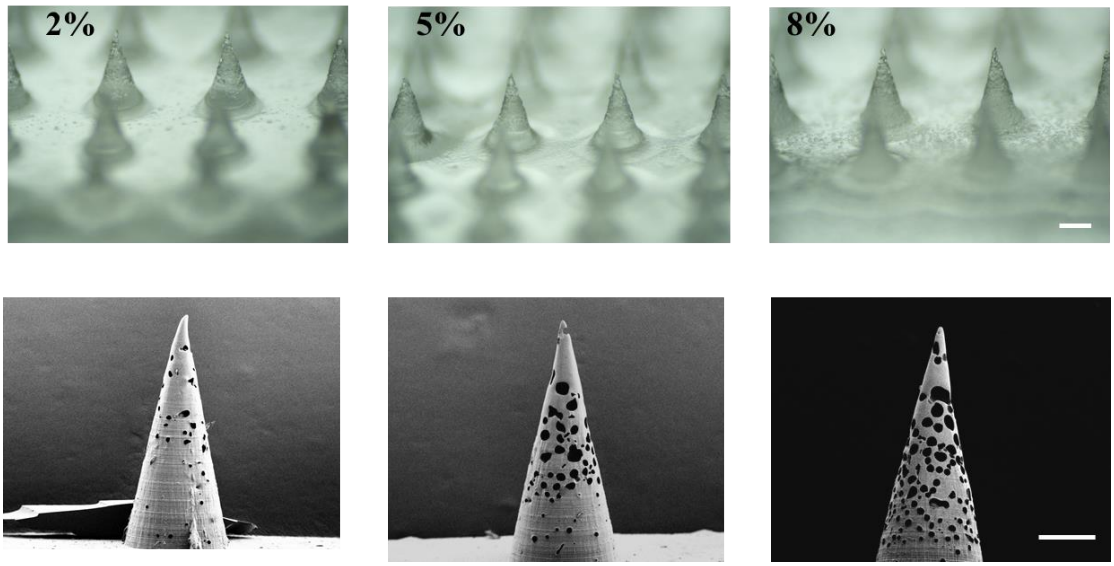

Figure S4. Optical images and SEM of porous MNs prepared with different concentration of SiO_2 glass spheres; both scale bars are 200 μm.

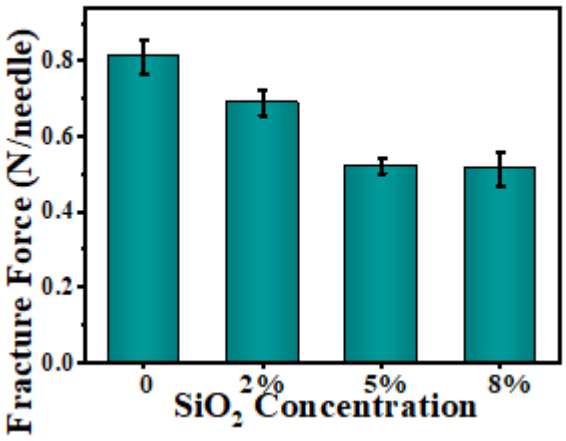

Figure S5. Fracture strength of the porous MN array with different concentrations of SiO_2 glass spheres. Data are presented as mean ± SD (n = 5).

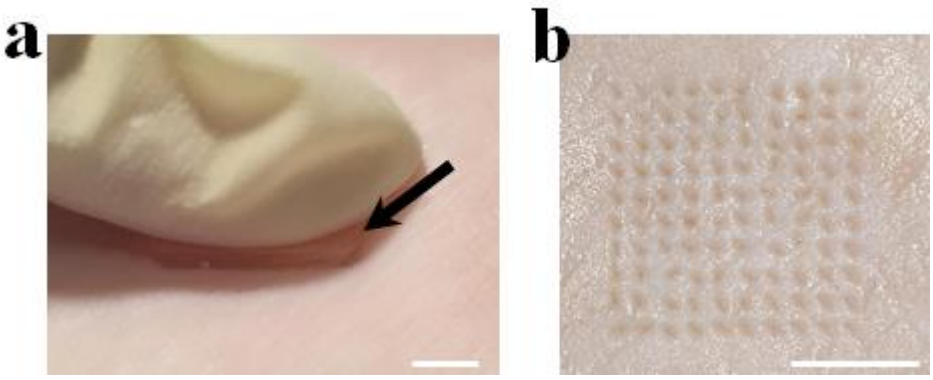

Figure S6. (a) Pressing the porous MNs to pigskin and (b) imprints left on the pigskin surface after MNs insertion. The arrow indicated the MN patch. Both Scale bars are 5 mm.

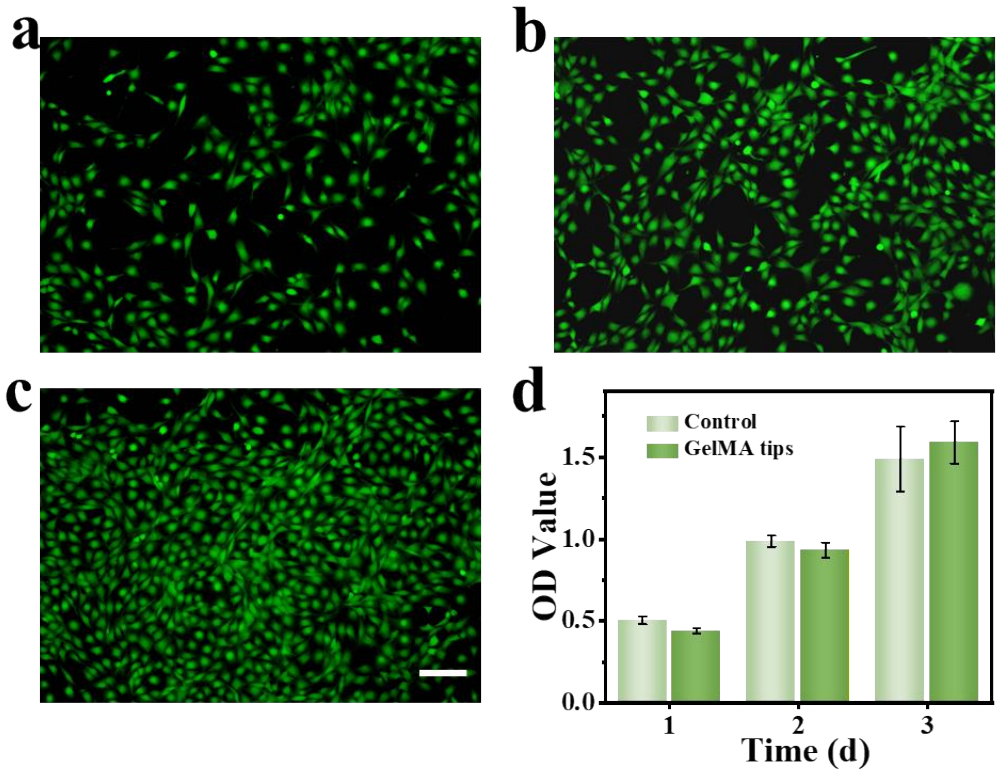

Figure S7. 3T3 cell proliferation in control and GelMA group during 3 days; scale bar is 100 μm. Data are presented as mean ± SD (n = 5).

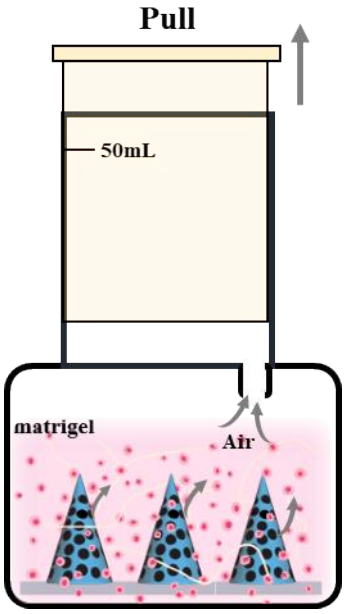

Figure S8. The device for porous MNs perfused with ADSCs.

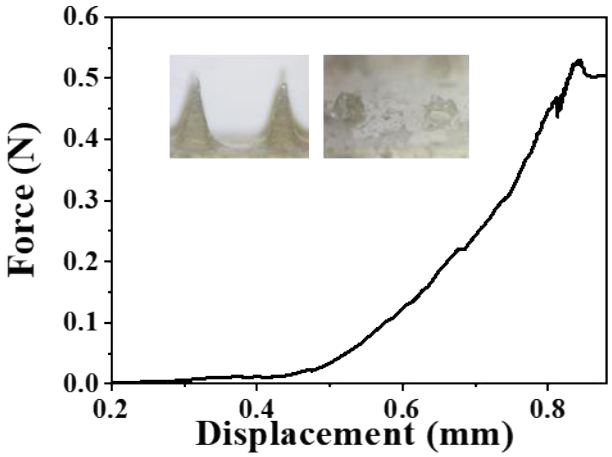

Figure S9. Mechanical strength of ADSCs-porous MNs.

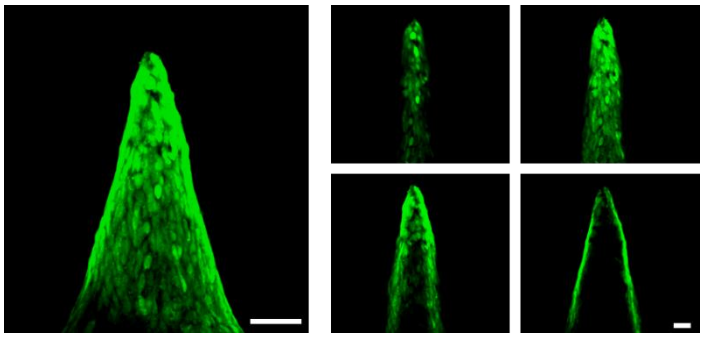

Figure S10. Fluorescence staining and layer scanning images of porous MNs perfused with 3T3 with higher initial cell loading amount; both scale bars are 100 μm.